Human-in-the-Loop Control of Soft Exosuits Using Impedance Learning on Different Terrains

Zhijun Li, *Fellow, IEEE*, Xiang Li, Qinjian Li, Hang Su, *Member, IEEE*, Zhen Kan, *Member, IEEE*, and Wei He, *Senior Member, IEEE*

***Abstract*—Many previous works of soft wearable exoskeletons (exosuit) target at improving the human locomotion assistance, without considering the impedance adaption to interact with the unpredictable dynamics and external environment, preferably outside the laboratory environments. This article proposes a novel hierarchical human-in-the-loop paradigm that aims to produce suitable assistance powers for cable-driven lower limb exosuits to aid the ankle joint in pushing off the ground. It includes two primary loop layers: impedance learning in the external loop and human-in-the-loop adaptive management in the inner loop. Considering unknown terrains, its impedance model can be transferred to a quadratic programming problem with specified constraints, which a designed primal-dual optimization prototype then solves. Then, the presented impedance learning strategy is introduced to regulate the impedance model with the adaptive assistant powers for humans on different terrains. An adaptive controller is designed in the inner loop to balance the nonlinearities and compliance existing in the human-exosuit coexistence, while the robust mechanism compensates for disturbances to facilitate trajectory management without employing the general regressor. The advantage of the proposed technique over conventional solutions with fixed impedance parameters is that it can improve human walking performance over different terrains. Experiments demonstrate the significance of the approach.**

***Index Terms*—Human-in-the-loop adaption, impedance learning, soft exosuit.**

Manuscript received 31 October 2021; revised 9 February 2022; accepted 3 March 2022. Date of publication 22 April 2022; date of current version 4 October 2022. This work was supported in part by the National Key Research and Development Program of China under Grant 2021YFF0501600 and Grant 2018YFC2001602, in part by the Major Science and Technology Projects of Anhui Province under Grant 202103a05020004, and in part by the National Natural Science Foundation of China under Grant U1913601 and Grant U2013601. This article was recommended for publication by Associate Editor Chenguang Yang and Editor Eiichi Yoshida upon evaluation of the reviewers' comments. *(Corresponding author: Wei He.)*

Zhijun Li, Xiang Li, and Qinjian Li are with the Department of Automation, University of Science and Technology of China, Hefei 230026, China, and also with the Institute of Artificial Intelligence, Hefei Comprehensive National Science Center, Hefei 230088, China (e-mail: zjli@ieee.org; lx2019@mail.ustc.edu.cn; lqj0414@mail.ustc.edu.cn).

Hang Su is with the Department of Electronics, Information and Bioengineering, Politecnico di Milano, 20133 Milan, Italy (e-mail: hang.su@ieee.org).

Zhen Kan is with the Department of Automation, University of Science and Technology of China, Hefei 230026, China.

Wei He is with the Institute of Artificial Intelligence, University of Science and Technology Beijing, Beijing 100083, China, and also with the School of Automation and Electrical Engineering, University of Science and Technology Beijing, Beijing 100083, China (e-mail: weihe@ieee.org).

Color versions of one or more figures in this article are available at https://doi.org/10.1109/TRO.2022.3160052.

Digital Object Identifier 10.1109/TRO.2022.3160052

I. Introduction

OVER the last decades, wearable robotic exoskeletons have been implemented in various scenarios, such as, assisting human walk, empowering human strength and endurance, and helping the patient in various medical rehabilitation scenarios [1]–[3]. However, most existing exoskeletons are with rigid structures, which can reduce the human body's load and energy expenditure by transferring the body's weight to the ground during human walking [4]–[7]. Due to the shortcoming of high inertia and joint alignment problems [8], the exoskeleton with rigid structures significantly increases the wearers net metabolic rate. The main challenges existing are that partial assistance by exoskeleton in the real world is more universal than complete support by rigid-bodied exoskeleton in the laboratory, leading to transitions toward compliant, portable, and wearable systems. Hence, an exoskeleton with soft lower limb, named soft exosuit, has been designed to handle the challenge in human walking assistance [9]. Compared with traditional rigid exoskeletons, the proposed soft exosuit adopts the flexible wire-driven mode to transfer the tension through the contraction line distance, which is featured of lightweight, small size, and high flexibility [10]. For wire-driven lower limb soft exosuits, electrical driver such as motors and controllers can be placed in the appropriate load-bearing part of the human body to reduce the robot system's adverse impact on the daily activities of the user wearing the exoskeleton. Due to these advantages, the research on design of soft exosuits has attracted tremendous popularity [11]–[13] (shown in Table I). Different from previous related works, this article considers the interaction model between human and environment to meet the fundamental control requirements of soft exosuits for assisting human to walk on different terrains.

Due to physical human–robot interaction, the users wearing flexible exoskeletons must interact effectively with the environment when walking on different terrains. Walking on natural and complex terrain consumes more energy than walking on hard and flat ground for human. Many factors affect gait biomechanics and energy consumption, such as terrain roughness, damping, stiffness, and friction [14]. In [15], it is pointed out that the energy consumption of walking on the beach is 2.1–2.7 times higher than that of walking on the flat ground, which is caused by the fact that muscles and tendons do positive work, while the mechanical work doing in the sand is less efficient. However, humans can easily switch between different walking gaits to compensate for force variants and instabilities in the dynamic surrounding environment when walking on

TABLE I
RELATED WORKS OF EXOSUITS

	Related Works	Difference/Demerit
[11]	Ankle passive powered exoskeleton using energy conversion and flexible transmission.	Not consider the interaction between exoskeleton and environment.
[12]	Portable and hingeless knee flexible exoskeleton using multi-point reference trajectory generator.	Only tested in a laboratory environment.
[13]	Ankle flexion aid exoskeleton without protruding parts from shoes, legs, waist or back.	Cannot adapt to the complex and dynamic environment.
[30]	Harvard exosuit with a force-based position controller.	Cannot adapt to walking on the different terrains.
[31], [32]	Exploiting admittance-based force tracking for the uppper/lower limbs.	Imposed strict requirements on the design of the control approach.

different terrains. Up to date, exoskeleton robots still lack such adaptability and are generally not capable of handling unstable interactions. These unknown impedance parameters can lead to the unstable interaction between the soft exosuit robot and the natural complex terrain. Therefore, this article designs a novel iterative learning controller based on the existing platform's impedance model to adapt to these unknown impedance parameters.

The human central nervous system has been shown to be able to efficiently adjust limb movements and impedance in dynamic environments with uncertain internal dynamics [16], [17]. Thus, the application of human learning skills to robotic control has become attractive [18]. It has been demonstrated that the human body will automatically adjust the limb impedance in different environments. The parameters of the target impedance model can be adapted by certain learning methods [19], [20], [49]. Kim *et al.* [21] adopted the equilibrium point control model to learn the stiffness parameter by using the natural actor-critic algorithm according to different application requirements. Yang *et al.* [22] presented a framework that the human tutor's movement and stiffness features can be actively learned by robot. In [23], a sensorless admittance control scheme was presented for the situation where robotic manipulators interacted with unknown environments even if the actuator saturation appeared. However, the aforementioned learning methods utilize traditional adaptive techniques to describe/estimate the dynamics of the environment, which is complicated. Compared with the aforementioned works, to learn a target impedance model, we first formulate the impedance learning as a cost function, and then, a novel optimization model is used to obtain an target impedance model, which can simultaneously adjust the stiffness and damping matrix and facilitate the convergence to the optimal values.

After obtaining the exact impedance parameters through the optimization model, to apply the modeled impedance data on the soft exosuit, we need to develop two main layers: the impedance learning in the outside loop combines with the position control in the inner control loop [49]. Impedance learning is utilized to handle the virtual reference trajectory with this approach. Next, the position control loop is applied to track the virtual reference trajectory. Proportional derivative (PD) control can be designed to guarantee the closed-loop scheme stability where the designed PD gains might regulate. However, the performance of PD control is sensitive to the unknown dynamics. In previous works [24], [25], [26], adaptive control has been widely studied in parametric and nonparametric uncertain control [27], [28]. In [27], neural adaptive control was proposed by introducing the neural-network-based function regressor with linear-in-the-parameter technique. In [28], adaptive control was presented with the robust featured regressor and the adaptive parameter adaption. The control design has been slightly improved by responding to the partial dynamics model. Although the adaptive control discussed previously can achieve better tracking performance, robots' dynamic information is indispensable and would lead to hurdles in actual implementation.

The control of human-in-the-loop allows soft exosuit to be involved in human locomotion actively and can provide necessary assistance and support for the human-exosuit walking on the different terrains. The assistance of lower limbs is another challenge that involves multiple joints across multiple task dimensions [29]. Within the human-in-the-loop framework, soft exosuit is involved in the human locomotion loop and preforms share control to fulfill a given task. A successful paradigm can be found in [30]–[32] (shown in Table I). Previous proposed controllers, for example, do not consider and regulate the magnitude of assistance, even if the varying walking speeds, terrains, and carried loads might demand different dynamics. To our best knowledge, up to date, few works can discern and adapt to walking on the different terrains. The deficiency of adaptability capacity restricts the usefulness of the exoskeleton, which can result in limited activities of the user, and in the worst case, a fall [33].

Considering the aforementioned difficulties, a novel hierarchical human-in-the-control scheme for cable-driven lower limb exosuits is addressed in this article. This solution is capable of dealing with impedance learning, adaption, and locomotion reference tracking with the nonlinearities and compliance existing in the human-exosuit interaction so that practical walking assistance on the terrains can be performed. First, the proposed scheme consists of two main layers: the impedance learning in the external loop and the human-in-the-loop adaptive control in the inner loop. Taking into account the unknown terrains, its impedance model can be transferred to a quadratic programming (QP) problem with specified constraints, which is addressed using a designed primal-dual optimization. Then, the proposed impedance learning can adapt the impedance model to regulate the assistance forces for humans walking on different terrains. Adaptive control is exploited in the inner loop to balance the nonlinearities and compliance existing in the human-exosuit interaction, while the robust mechanism balances the disturbances. Compared with the conventional impedance solution with designated impedance parameters, the benefit of the presented technique is that it can accomplish more satisfactory performance for humans walking on different terrains. Extensive experiments

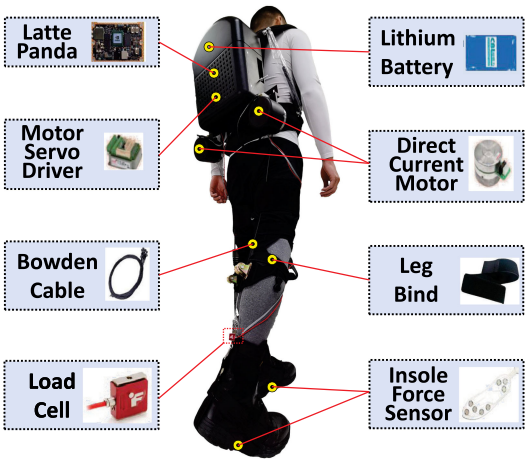

Fig. 1. Developed soft exosuit.

have been performed to demonstrate the significance of the technique.

The main contributions of this article are as follows.

1) A kinematic model of human and exosuit is first proposed, where the geometry relation between the human ankle joints and the exosuit drive joints are formulated.
2) Using QP based on a prime-dual model, impedance learning has been proposed to adaptively adjust the impedance parameters of the exosuit so that the desired impedance model can be obtained in the case of unknown terrains.
3) A human-in-the-loop adaptive control scheme is developed for walking on different terrains with varying speeds and carried loads. Theoretical analysis and experimental locomotion tests have been performed.

II. System Overview

A. Exosuit Platform

A soft exosuit platform shown in Fig. 1 is developed to assist the human locomotion. Two brushless dc motors at the waist (160 Watt, Maxon EC 90 flat plate) with integrated harmonic reducer (SHD-14-100-2SH) deliver torque to the wearer's ankle via Bowden cables. Two load cells (LSB201, FUTEK Advanced Sensor Technology, Inc.,CA, USA) measure tension forces that are applied between the exosuit components. An embedded circuit board is fixed on the waist belt, which is integrated with motor servo-controllers, drivers, sensor connectors, a Lithium Polymer battery (24 V, 17.5 Ah), and a microcontroller. The specification parameters of the insole force sensor and the load cell (LSB201) are shown in Tables II and III, respectively.

B. Human-Exosuit Kinematics and Dynamics

From Figs. 2 and 3, the geometry relationship between the ankle joint angular position $q \in \mathbb{R}$ and the exosuit joint angular position $q_h \in \mathbb{R}$ can be described by

$$r_h(q_h - q_0) = \sqrt{l_a^2 + r_a^2 - 2l_a r_a \cos\alpha} - \sqrt{l_a^2 + r_a^2 - 2l_a r_a \cos(\alpha - q)} \quad (1)$$

TABLE II
Specifications of Insole Force Sensor

Parameters	Value
Range(Single Point)	10 kg
Thickness	< 0.45 mm
Size	41 yards
Minimum Response	400 g
No Load Resistance	$> 10M\Omega$
Maximum Response time	< 1 ms
Excitation Voltage	DC 3.3 V
Temperature	$-20 \sim 60°C$

TABLE III
Specifications of Load Cell

Parameters	Value
Metre Full Scale	100 lb
Weight	22.6 g
Rated load	45, 359.24 g
Sensitivity	$1 - 2$mV/V
Nonlinearity	0.1% F.S
Deformation Quantity	$0.07 - 0.12$ mm
Operating Temperature	$-50 \sim 93°C$
Nominal Voltage	5 VDC

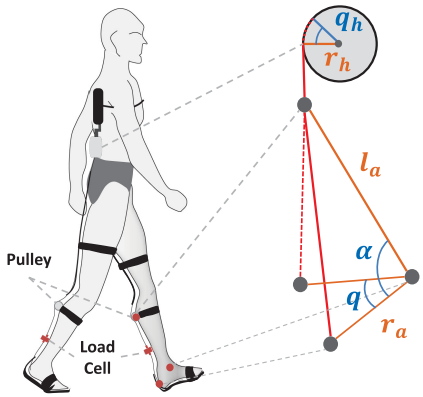

Fig. 2. Geometric relationship between the exosuit joint on the waist and the human ankle joint.

where q_0 is the initial value of q, q is the output angle of the driven motor, r_h is the radius of the exosuit joint output shaft, which is worn on the human waist, l_a is the distance between the ankle joint center and the pulley on the shank, r_a represents the distance between the ankle joint center and the pulley on the heel of the same leg, and α is the initial angle of the ankle joint. The human ankle joint is simplified to be rotated with respect to a single and fixed center of rotation, inspired by [34]–[37]. Therefore, the ankle angle is simplified as rotating to a single joint.

Taking the time derivative of (1) yields

$$r_h \dot{q}_h = \dot{q} \frac{r_a l_a \sin(\alpha - q)}{\sqrt{r_a^2 + l_a^2 - 2r_a l_a \cos(\alpha - q)}}. \quad (2)$$

Then, (2) can be rewritten as

$$\dot{q} = \dot{q}_h \frac{(\lambda(q))^{\frac{1}{2}} r_h}{r_a l_a \sin(\alpha - q)} \quad (3)$$

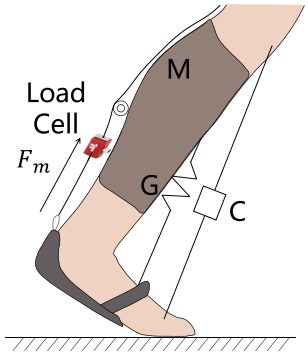

Fig. 3. Model of the human ankle.

where $\lambda(q) = r_a^2 + l_a^2 - 2r_a l_a \cos(\alpha - q)$.

Take the derivative of (3) with respect to time as

$$\ddot{q} = \left[\dot{q}_h \left(-\dot{q}\lambda(q)^{-\frac{1}{2}} + \frac{\lambda(q)^{\frac{1}{2}}\cos(\alpha - q)}{r_a l_a \sin^2(\alpha - q)}\right) + \ddot{q}_h \frac{\lambda(q)^{\frac{1}{2}}}{r_a l_a \sin(\alpha - q)}\right] r_h.$$

Hence, we have

$$\dot{q} = J(q)\dot{q}_h \tag{4}$$

$$\ddot{q} = Q(q,\dot{q})\dot{q}_h + J(q)\ddot{q}_h \tag{5}$$

where $J(q) = \frac{(\lambda(q))^{\frac{1}{2}} r_h}{r_a l_a \sin(\alpha - q)}$, and $Q(q,\dot{q}) = (-\dot{q}\lambda(q)^{-\frac{1}{2}} + \frac{\lambda(q)^{\frac{1}{2}}\cos(\alpha-q)}{l_a r_a \sin^2(\alpha-q)})r_h$. Fig. 2 illustrates that the Bowden cables are tightened and inelastic when assisting plantar flexion, which can transmit the force from the exosuit joints to the wearer's ankle joints through a pulley on the calf, and the Bowden cables go through the pulley and connect to the shoes.

Considering the joints of the exosuit and human ankle, the exosuit dynamics can be described as

$$M(q)\ddot{q} + C(q,\dot{q})\dot{q} + \tau_f(\dot{q}) + G(q) = \tau_m - F_m \tag{6}$$

with the inertia matrix $M(q) \in \mathbb{R}^{n\times n}$ with $n = 2$, the nonlinear term matrix of Coriolis and Centrifugal forces $C(q,\dot{q}) \in \mathbb{R}^{n\times n}$, the gravitational forces vector $G(q) \in \mathbb{R}^n$, the joint variables $q = [q_l, q_r]^T \in \mathbb{R}^n$, the external disturbance $\tau_f = [\tau_{fl}, \tau_{fr}]^T \in \mathbb{R}^n$ representing the matrix composed of damping friction for each joint, the control input $\tau_m = [\tau_{m_l}, \tau_{m_r}]^T \in \mathbb{R}^n$, and the interaction force between the human ankle and the motor $F_m = [F_{m_l}, F_{m_r}]^T \in \mathbb{R}^n$. In the aforementioned formula, the subscript l is the parameter of the left ankle, and the subscript r is the parameter of the right ankle.

Then, the following properties in [38]–[41], and [48] would be used to design the controller and analyze the stability of the dynamics (6).

Property 1: M(q) in (6) is positive definite symmetric, with the following property:

$$m_1\|\xi\|^2 \le \xi^T M(q)\xi \le m_2\|\xi\|^2 \quad \forall \xi \in \mathbb{R}^n \tag{7}$$

where $\|\cdot\|$ is the standard Euclidean norm and m_1 and m_2 are known positive constants.

Property 2: $\|C(q,\dot{q})\| \le k_C\|\dot{q}\|$, $\|G(q)\| \le k_G$, $\|M(q)\| \le k_M$, where k_C, k_G, and k_M are unknown positive scalars.

Property 3: $M(q)$ and $C(q,\dot{q})$ have the following skew symmetric property:

$$\xi^T\left(\frac{1}{2}\dot{M}(q) - C(q,\dot{q})\right)\xi = 0 \quad \forall \xi \in \mathbb{R}^n. \tag{8}$$

Property 4: The dynamics of (6) can be written in a linear form

$$\psi_d(q,\dot{q},\ddot{q})\theta_d = M(q)\ddot{q} + C(q,\dot{q})\dot{q} + G(q) \tag{9}$$

where $\theta_d \in \mathbb{R}^p$ is a constant matrix that contains the parameters of physics system, and the matrix $\psi_d(q,\dot{q},\ddot{q}) \in \mathbb{R}^{n\times p}$ is a known function that contains q, $\dot{q}$, and $\ddot{q}$.

Property 5: For all $\xi, \nu \in \mathbb{R}^n$, we have

$$C(q,\xi)\nu = C(q,\nu)\xi. \tag{10}$$

Property 6: The $\tau_f(\dot{q})$ is usually treated as two items including viscous and Coulomb friction as

$$\tau_f(\dot{q}) = f_v\dot{q} + f_c\mathrm{sgn}(\dot{q}) \tag{11}$$

with the viscous friction coefficient $f_v = \mathrm{diag}[f_{v1}, \ldots, f_{vn}]$ and the coefficient of Coulomb friction $f_c = \mathrm{diag}[f_{c1}, \ldots, f_{cn}]$, $\mathrm{sgn}(\cdot)$ is the sign function. The friction $\tau_f(\dot{q})$ can be linearly parameterized as

$$\tau_f(\dot{q}) = \psi_f(q,\dot{q},\ddot{q})\theta_f \tag{12}$$

where θ_f denotes the parameter of friction, which is unknown or to be estimated online.

From Properties 4 and 6, one obtains

$$\psi(q,\dot{q},\ddot{q})\theta = M(q)\ddot{q} + C(q,\dot{q})\dot{q} + \tau_f(\dot{q}) + G(q) \tag{13}$$

where $\psi(q,\dot{q},\ddot{q}) = \mathrm{diag}[\psi_d(q,\dot{q},\ddot{q}), \psi_f(q,\dot{q},\ddot{q})]$, and $\theta = [\theta_d, \theta_f]^T$.

Property 7: To help the subsequent control design and analysis, it can be shown that the following equalities/inequalities [48] hold $\forall x = [x_1, \ldots, x_n]^T \in \mathbb{R}^n$, we have

$$\tanh(x) = [\tanh(x_1), \ldots, \tanh(x_n)]^T$$

$$\|x\| \ge \|\tanh(x)\|$$

$$\|x\|^2 \ge \sum_{i=1}^{n} \ln(\cosh(x_i)) \ge \ln(\cosh(\|x\|)) \ge \frac{1}{2}\tanh^2(\|x\|)$$

$$x^T\tanh(x) \ge \|\tanh(x)\|^2 \ge \tanh^2(\|x\|)$$

$$\|x\| + 1 \ge \frac{\|x\|}{\tanh(\|x\|)}.$$

C. Control Objective

In the article, considering the impedance characteristics between the human foot and the contact ground during human locomotion, we exploit a mass–damper–spring model as $M_d(\ddot{q}_d - \ddot{q}_r) + C_d(\dot{q}_d - \dot{q}_r) + G_d(q_d - q_r) = F_m$, where

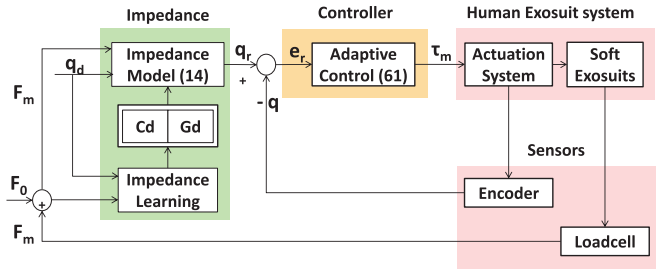

Fig. 4. Control structure.

$M_d = \mathrm{diag}[m_{d_l}, m_{d_r}] \in \mathbb{R}^{n\times n}$, $C_d = \mathrm{diag}[c_{d_l}, c_{d_r}] \in \mathbb{R}^{n\times n}$, and $G_d = \mathrm{diag}[g_{d_l}, g_{d_r}] \in \mathbb{R}^{n\times n}$ denote the human left and right ankles' inertia, damper, and stiffness matrix, respectively; $q_d \in \mathbb{R}^n$ denotes the desired ideal trajectories of the left and right ankles, $q_r = [q_{r_l}, q_{r_r}]^T \in \mathbb{R}^n$ is the reference trajectories of the left and right ankles, and $F_m \in \mathbb{R}^n$ is the measured cable forces for the left and right ankles. From [42], since the impedance model mainly depends on the spring and damper components, it can be simplified as

$$C_d(\dot{q}_d - \dot{q}_r) + G_d(q_d - q_r) = F_m \tag{14}$$

where C_d and G_d are unknown. From (14), the reference trajectory q_r is difficult to obtain, even if F_m can be measured by a force sensor. Therefore, the impedance parameters C_d and G_d should be estimated.

The designed controller delivers a hierarchical configuration, beginning by evaluating the assistance efforts inquired by the user and ending with the piece of the movement passed to the joint during the transmission of the tendon. The scheme design in Fig. 4 contains two layers: an outer loop and an inner loop. The purpose of the outer loop is to acquire the impedance parameters C_d and G_d of the external environment and unpredictable dynamics, and consequently, provides a practical reference motion q_r of human angle joints. At the same time, the inner loop controller is dedicated to following the reference trajectory correctly. The inconsistent and nonlinearities inherent in the slack of the Bowden cable introduce significant time delay and inaccuracy in trajectory tracking. Thus, the motion required in the actuation phase is transmitted to the inner controller, which calculates the torque τ_m and transits it to the motor to enhance the control accuracy in an effective way, balance the friction, and deliver an additional torque for the whole procedure.

III. Impedance Learning

The measured cable force F_m in (14) can be rewritten as

$$F_m = G_d q_d + C_d \dot{q}_d - F_0 \tag{15}$$

where $F_0 = G_d q_r + C_d \dot{q}_r$, G_d and C_d are the desired values. Considering the estimation values of G_d and C_d, we have

$$\hat{F}_m = \hat{G}_d q_d + \hat{C}_d \dot{q}_d - \hat{F}_0 \tag{16}$$

where $\hat{F}_0 = \hat{G}_d q_r + \hat{C}_d \dot{q}_r$. From (15) and (16), we can obtain

$$\tilde{F}_m = \tilde{G}_d q_d + \tilde{C}_d \dot{q}_d - \tilde{F}_0 \tag{17}$$

where $\tilde{G}_d = \hat{G}_d - G_d$, $\tilde{C}_d = \hat{C}_d - C_d$, $\tilde{F}_m = \hat{F}_m - F_m$, and $\tilde{F}_0 = \hat{F}_0 - F_0$.

Considering (17), we try to minimize $\tilde{F}_m$ and formulate the following QP problem as

$$\min \quad \frac{1}{2}\chi^T W \chi \tag{18}$$

$$\text{s.t.} \quad \mathcal{R}\chi = \tilde{F}_m + \tilde{F}_0 \tag{19}$$

$$\chi^- \le \chi \le \chi^+ \tag{20}$$

where the vector and coefficient matrix involved are defined as $\chi = [\tilde{\mathcal{C}}_d^T, \tilde{\mathcal{G}}_d^T]^T \in \mathbb{R}^N$ with $N = 4$, $\tilde{\mathcal{C}}_d = [\tilde{c}_{d_l}, \tilde{c}_{d_r}]^T$, $\tilde{\mathcal{G}}_d = [\tilde{g}_{d_l}, \tilde{g}_{d_r}]^T$, $\chi^- = [\tilde{\mathcal{C}}_d^{-T}, \tilde{\mathcal{G}}_d^{-T}]^T \in \mathbb{R}^N$ is the lower bounds, $\chi^+ = [\tilde{\mathcal{C}}_d^{+T}, \tilde{\mathcal{G}}_d^{+T}]^T \in \mathbb{R}^N$ is the upper bounds, $W = \mathrm{diag}[W_c, W_k] \in \mathbb{R}^{N\times N}$ with the weighted parameters W_c and W_k, $\mathcal{R} = \mathrm{diag}[\dot{q}_d^T, q_d^T] \in \mathbb{R}^{n\times N}$, and $(\tilde{F}_m + \tilde{F}_0) \in \mathbb{R}^n$,

First, we transform QP in (18)–(20) into a set of linear variational inequalities. That is, to find a primal-dual equilibrium vector $y^* \in \Omega := \{\sigma | y^- \le \sigma \le y^+\}$ such that $\forall y \in \Omega$, the following equations (21)– (29) hold [43], [44]

$$(y - y^*)^T(\Phi y^* + \eta) \ge 0 \tag{21}$$

where $y \in \mathbb{R}^{(n+N)}$ denotes the primal-dual decision vector and we can define the lower and upper bounds as follows:

$$y = \begin{bmatrix} \chi \\ \rho \end{bmatrix}, y^- = \begin{bmatrix} \chi^- \\ -\varpi \end{bmatrix}, y^+ = \begin{bmatrix} \chi^+ \\ \varpi \end{bmatrix} \tag{22}$$

where $\rho \in \mathbb{R}^n$ denotes the dual decision vectors corresponding to equality constraint (19), and the augmented coefficient matrix $\Phi \in \mathbb{R}^{(n+N)\times(n+N)}$ and $\eta \in \mathbb{R}^{(n+N)}$ are defined as

$$\Phi = \begin{bmatrix} W & -\mathcal{R}^T \\ \mathcal{R} & \mathbf{0}_{n\times n} \end{bmatrix}, \eta = \begin{bmatrix} \mathbf{0_{N\times 1}} \\ -(\tilde{F}_m + \tilde{F}_0) \end{bmatrix}. \tag{23}$$

Then, a necessary and sufficient condition for the optimum point (χ^*, ρ^*) of the primal QP problem (18)–(20) is

primal feasibility:

$$\mathcal{R}\chi^* - (\tilde{F}_m + \tilde{F}_0) = 0$$
$$\chi^- \le \chi \le \chi^+;$$

dual feasibility:

$$W\chi^* - \mathcal{R}^T\rho^* = 0,$$
$$\rho^* \text{unrestricted}. \tag{24}$$

In addition, by defining $\Omega_1 = \{\chi | \chi^- \le \chi \le \chi^+\} \subset \mathbb{R}^N \forall \chi \in \Omega_1$, we have

$$(\chi_i - \chi_i^*)\begin{cases} \le 0, & \chi_i^* = \chi_i^+ \\ \in (\chi_i^- - \chi_i^+, \chi_i^+ - \chi_i^-), & \chi_i^* \in (\chi_i^-, \chi_i^+) \\ \ge 0, & \chi_i^* = \chi_i^-. \end{cases} \tag{25}$$

From the aforementioned equation, we can derive the following linear variational inequality (LVI), i.e., to find an $\chi^* \in \Omega_1$

such that

$$(\chi - \chi^*)^T \left(W\chi^* - \mathcal{R}^T\rho^*\right) \geq 0 \, \forall \chi \in \Omega_1. \tag{26}$$

Similarly, we can define $\Omega_2 = \{\rho | -\varpi \leq \rho \leq \varpi\} \in \mathbb{R}^N$. Therefore, we obtain the following LVI formulation for the equality constraint in (24), i.e., to find a $\rho^* \in \Omega_2$ such that

$$(\rho - \rho^*)(\mathcal{R}\chi^* - (\tilde{F}_m + \tilde{F}_0)) \geq 0 \qquad \forall \rho \in \Omega_2. \tag{27}$$

Finally, a set Ω can be defined by utilizing the Cartesian product as

$$\begin{aligned}\Omega &= \Omega_1 \times \Omega_2 \\ &= \left\{ y = \begin{bmatrix} \chi \\ \rho \end{bmatrix} \mid \begin{bmatrix} \chi^- \\ -\varpi \end{bmatrix} \leq \begin{bmatrix} \chi \\ \rho \end{bmatrix} \leq \begin{bmatrix} \chi^+ \\ \varpi \end{bmatrix} \right\} \\ &= \left\{ y \in R^{(n+N)} \mid y^- \leq y \leq y^+ \right\}. \end{aligned} \tag{28}$$

The linear variational inequalities scattered in (26) and (27) could be combined into a single LVI problem, i.e., to find $y^* \in \Omega$ such that $\forall y = [\chi^T, \rho^T]^T \in \Omega$ as

$$\begin{aligned}&\left(\begin{bmatrix} \chi \\ \rho \end{bmatrix} - \begin{bmatrix} \chi^* \\ \rho^* \end{bmatrix} \right)^T \\ &\left(\begin{bmatrix} W & -\mathcal{R}^T \\ \mathcal{R} & \mathbf{0}_{n\times n} \end{bmatrix} \begin{bmatrix} \chi^* \\ \rho^* \end{bmatrix} + \begin{bmatrix} \mathbf{0_{N\times 1}} \\ -(\tilde{F}_m + \tilde{F}_0) \end{bmatrix} \right) \geq 0. \end{aligned} \tag{29}$$

The aforementioned LVI (29) is equivalent to the QP problem (18)–(20). To solve (29), the following primal-dual model is considered [44]:

$$\dot{y} = -y + P_\Omega \left(y - (\Phi y^* + \eta) \right) \tag{30}$$

where $P_\Omega(\cdot)$ is the projection operator into Ω and defined as $P_\Omega(y) = [P_\Omega(y_1), \cdots, P_\Omega(y_{n+N})]^T$ with

$$P_\Omega(y_i) = \begin{cases} y_i^-, & \text{if } y_i < y_i^- \\ y_i, & \text{if } y_i^- \leqslant y_i \leqslant y_i^+ \\ y_i^+, & \text{if } y_i > y_i^+ \end{cases}$$

for $\forall i \in \{1, 2, \ldots, \varrho\}$, and $\varrho = n + N$. If y is an equilibrium point of the model (30), then

$$y = P_\Omega \left(y - (\Phi y^* + \eta) \right). \tag{31}$$

Therefore, a modified projection model can be chosen as [43], [44]

$$\dot{y} = \gamma(I + \Phi^T)\{P_\Omega \left(y - (\Phi y + \eta) \right) - y\} \tag{32}$$

where γ is used to measure the convergence rate of the system and is a strictly positive parameter, which should be carefully designed.

Remark 1: To solve QP (18), compared with a traditional QP method, for example, we choose the function "QUADPROG" in the MATLAB Optimization Toolbox, and the descent method is usually exploited, where the Hessian matrix of the Langragian is repeatedly calculated [45], [46], and the complexity of the traditional QP solution is $O(n^4 + n + (6N + 6n)N^2 + (7N + 6n)^3)$.

IV. Control Design

A. Preliminary: PD Control

The motivation of the exosuit control design is to enable desired assistance performance between soft exosuit and human. After C_d and G_d are obtained through the impedance learning process, the virtual reference trajectory can be solved by the impedance model (14). Thus, the control objective is to drive the position q to track the time-varying reference position q_r, while all the signals in the control system should be bounded.

First, the position control is proposed as follows:

$$\tau_m = K_p \tanh(e_r) + K_d \dot{e}_r + F_m \tag{33}$$

where $K_p \in \mathbb{R}^{n\times n}$ and $K_d \in \mathbb{R}^{n\times n}$ are positive constant diagonal matrices, and $e_r = q_r - q$ denotes the position tracking error, F_m is defined in (6).

Define an auxiliary variable as

$$r = -\dot{e}_r - \mu \tanh(e_r) \tag{34}$$

where $\mu \in \mathbb{R}^{n\times n}$ is a positive constant diagonal matrix.

Taking the derivative of (34) with respect to time, and multiplying both sides of the result by $M(q)$, and then, utilizing (6), we have

$$M(q)\dot{r} = -C(q, \dot{q})r + \psi_a\theta + \tau_m - F_m \tag{35}$$

where the linear parameterized term $\psi_a\theta$, as similar as (13), with $\psi_a \in \mathbb{R}^{n\times p}$ and $\theta \in \mathbb{R}^p$, can be described as

$$\begin{aligned}\psi_a\theta = &-M(q)\left(\ddot{q}_r + \mu \cosh^{-2}(e_r)\dot{e}_r\right) - \tau_f(\dot{q}) - G(q) \\ &- C(q, \dot{q})\left(\dot{q}_r + \mu \tanh(e_r)\right). \end{aligned} \tag{36}$$

Remark 2: Different from the previous work [48], the friction vector is considered in ψ_a, by exploiting Properties 1 and 5 and the definition (34), and we can conclude that

$$\|\psi_a\theta\| \leq \zeta_0\|e_r\| + \zeta_1\|r\| \tag{37}$$

where ζ_0 and ζ_1 are bounded positive constants, and they are related to the physical system of the soft exosuit.

After substituting (33) into (35), we have

$$M(q)\dot{r} = -C(q, \dot{q})r + \psi_a\theta + K_p \tanh(e_r) + K_d\dot{e}_r. \tag{38}$$

Theorem 1: The controller (33) ensures position tracking in the sense that $\lim_{t\to\infty} e_r(t) = 0$ if the controller gain K_p satisfies the following sufficient condition:

$$\begin{aligned}\lambda_{\min}\{\mu K_p\} > &\frac{\lambda_{\min}^2\{\mu K_d\}}{\zeta_2(\cosh^{-1}(\exp(\frac{\lambda_2}{\lambda_1}\|z(0)\|^2) + 1)^2} \\ &+ \frac{{\zeta_0}^2(\cosh^{-1}(\exp(\frac{\lambda_2}{\lambda_1}\|z(0)\|^2) + 1)^2}{\zeta_2} \\ &- \frac{\lambda_{\min}\{\mu K_d\}\zeta_0}{2\zeta_2(\cosh^{-1}(\exp(\frac{\lambda_2}{\lambda_1}\|z(0)\|^2) + 1)} \end{aligned} \tag{39}$$

where $\zeta_2 = K_d - \zeta_1$, $z = [{e_r}^T, r^T]^T$, $z(0)$ is the initial value of z, and λ_1 and λ_2 are positive scalar constants that are selected as $\lambda_1 = \min\{\lambda_{\min}\{K_p\}, \frac{m_1}{2}\}$, $\lambda_2 = \max\{\lambda_{\max}\{K_p\}, \frac{m_2}{2}\}$, with $\lambda_{\min}\{\cdot\}$ denotes the minimum eigenvalues of a matrix, and $\lambda_{\max}\{\cdot\}$ denotes the maximum eigenvalues of a matrix.

Proof: Considering the following Lyapunov function candidate [48]:

$$V_1(t) = \frac{1}{2} r^T M(q) r + \sum_{i=1}^{n} k_p^i \ln(\cosh(e_r^i)) \tag{40}$$

where k_p^i is the ith diagonal element of the control gain K_p defined in (33), and e_r^i is the ith element of the vector e_r. Based on Properties 1 and 7, we have

$$\frac{1}{2} m_1 \ln(\cosh(\|r\|)) \leq \frac{1}{2} m_1 \|r\|^2 \leq \frac{1}{2} r^T M(q) r \leq \frac{1}{2} m_2 \|r\|^2 \tag{41}$$

$$\lambda_{\min}\{K_p\} \frac{1}{2} \ln(\cosh(\|e_r\|)) \leq \sum_{i=1}^{n} {k_p}^i \ln(\cosh(e_r^i)) \leq \lambda_{\max}\{K_p\} \|e_r\|^2. \tag{42}$$

After substituting (41) and (42) into (40), and letting $\mathcal{Y} = [{e_r}^T, r^T]^T$, we can obtain that $V_1(t)$ is bounded and satisfies the inequalities as

$$\begin{aligned} V_1(t) &\geq \frac{1}{2} m_1 \ln(\cosh(\|r\|)) + \sum_{i=1}^{n} \frac{1}{2} k_p^i \ln(\cosh(\|e_r^i\|)) \\ &\geq \frac{1}{2} \lambda_1 \ln(\cosh(\|r\|)) + \frac{1}{2} \lambda_1 \ln(\cosh(\|e_r\|)) \\ &\geq \frac{1}{2} \lambda_1 \ln(\cosh(\|\mathcal{Y}\|)) \geq \frac{1}{2} \lambda_1 \tanh^2(\|\mathcal{Y}\|) \end{aligned} \tag{43}$$

and

$$\begin{aligned} V_1(t) &\leq \frac{1}{2} m_2 \|r\|^2 + \lambda_{\max}\{K_p\} \|e_r\|^2 \\ &\leq \frac{1}{2} \lambda_2 \|r\|^2 + \lambda_2 \|e_r\|^2 \\ &\leq \lambda_2 \|r\|^2 + \lambda_2 \|e_r\|^2. \end{aligned} \tag{44}$$

And then utilizing (43), (44) can be simplified as

$$\begin{aligned} \frac{1}{2} \lambda_1 \tanh^2(\|\mathcal{Y}\|) &\leq \lambda_1 \ln(\cosh(\|\mathcal{Y}\|)) \\ &\leq V_1(t) \\ &\leq \lambda_2 (\|r\|^2 + \|e_r\|^2). \end{aligned} \tag{45}$$

Based on the first lower bound of $V_1(t)$ from (45), we can obtain that

$$\|\mathcal{Y}\| \leq \cosh^{-1}\left(\exp\left(\frac{V_1}{\lambda_1}\right)\right). \tag{46}$$

After taking the time derivative of (40), it is easy to have

$$\dot{V}_1(t) = r^T M(q) \dot{r} + \frac{1}{2} r^T \dot{M}(q) r + \tanh^T(e_r) K_p \dot{e}_r. \tag{47}$$

After substituting (38) for $M(q)\dot{r}$, the following equation can be obtained by utilizing Property 3 and eliminating the common items

$$\begin{aligned} \dot{V}_1(t) = & -\tanh^T(e_r) \mu K_p \tanh(e_r) - r^T \mu K_d \tanh(e_r) \\ & - r^T K_d r + r^T \psi_a \theta. \end{aligned} \tag{48}$$

Then, the following equations can be calculated. The upper bound of (48) can be formulated as

$$\begin{aligned} \dot{V}_1(t) \leq & -\lambda_{\min}\{\mu K_p\} \tanh^2(\|e_r\|) \\ & - \lambda_{\min}\{\mu K_d\} \tanh(\|e_r\|) \tanh(\|r\|) \\ & + \|r\| \|\psi_a \theta\|. \end{aligned} \tag{49}$$

Moreover, by utilizing (37), the upper bound of the last term of (49) can be written as follows:

$$\|r\| \|\psi_a \theta\| \leq \zeta_0 \|e_r\| \|r\| + \zeta_1 \|r\|^2. \tag{50}$$

Hence, the upper bound of $\dot{V}_1(t)$ can be further obtained as

$$\dot{V}_1(t) \leq -x^T Q x \tag{51}$$

where $x = [\tanh(\|e_r\|), \tanh(\|r\|)]^T \in \mathbb{R}^2$ and $Q \in \mathbb{R}^{2\times 2}$ are explicitly defined as follows:

$$Q = \begin{bmatrix} \lambda_{\min}\{\mu K_p\} & \\ \lambda_{\min}\{\mu K_d\} - \zeta_0 \frac{\|r\| \|e_r\|}{\tanh(\|r\|) \tanh(\|e_r\|)} & \\ \lambda_{\min}\{\mu K_d\} - \zeta_0 \frac{\|r\| \|e_r\|}{\tanh(\|r\|) \tanh(\|e_r\|)} & \zeta_2 \frac{\|r\|^2}{\tanh^2(\|r\|)} \end{bmatrix}. \tag{52}$$

In order to make the aforementioned matrix Q positive definite, both the sequential principal minor and the determinant should be greater than 0, thus the following inequalities must be satisfied:

$$\lambda_{\min}\{\mu K_p\} > 0 \tag{53}$$

$$K_d - \zeta_1 > 0 \tag{54}$$

and

$$\begin{aligned} \lambda_{\min}\{\mu K_p\} > & \frac{\lambda_{\min}^2\{\mu K_d\} \tanh^2(\|r\|)}{\zeta_2 \|r\|} + \frac{{\zeta_0}^2 \|e_r\|^2}{\zeta_2 \tanh^2(\|e_r\|)} \\ & - \frac{\lambda_{\min}\{\mu K_d\} \zeta_0 \|e_r\| \tanh(\|r\|)}{2\zeta_2 \tanh(\|e_r\|) \|r\|}. \end{aligned} \tag{55}$$

The sufficient condition of (55) can be developed as follows:

$$\begin{aligned} \lambda_{\min}\{\mu K_p\} > & \frac{\lambda_{\min}^2\{\mu K_d\}}{\zeta_2 (\|\mathcal{Y}\| + 1)^2} + \frac{{\zeta_0}^2 (\|\mathcal{Y}\| + 1)^2}{\zeta_2} \\ & - \frac{\lambda_{\min}\{\mu K_d\} \zeta_0}{2\zeta_2 (\|\mathcal{Y}\| + 1)}. \end{aligned} \tag{56}$$

Therefore, the sufficient condition for (56) can be described as follows:

$$\begin{aligned} \lambda_{\min}\{\mu K_p\} > & \frac{\lambda_{\min}^2\{\mu K_d\}}{\zeta_2 (\cosh^{-1}(\exp(\frac{V_1}{\lambda_1}) + 1)^2} \\ & + \frac{{\zeta_0}^2 (\cosh^{-1}(\exp(\frac{V_1}{\lambda_1}) + 1)^2}{\zeta_2} \\ & - \frac{\lambda_{\min}\{\mu K_d\} \zeta_0}{2\zeta_2 (\cosh^{-1}(\exp(\frac{V_1}{\lambda_1}) + 1)}. \end{aligned} \tag{57}$$

If (57) is established, due to Property 7, $\dot{V}_1(t)$ becomes

$$\dot{V}_1(t) \leq -\beta_1 \tanh^2(\|\mathcal{Y}\|) \leq 0 \tag{58}$$

where β_1 is some positive constant related to Q in (51). Hence, from (58), it is obtained that

$$V_1(z(t),t) \leq \lambda_2(\|r(0)\|^2 + \|e_r(0)\|^2). \tag{59}$$

The aforementioned results use the upper bound of inequality (45). Therefore, by using (59), the sufficient condition of (57) can be written in the form of (39). ■

B. Human-in-the-Loop Adaptive Control

Remark 3: "Human-in-the-loop adaptive control" describes that the impedance characteristics between the human foot and the contact ground during human locomotion can be exploited as the time-varying reference trajectory q_r in the adaptive control loop. Specifically, C_d and G_d in the impedance model (14) are adaptively adjusted using the proposed impedance learning approach despite unknown terrains. In order to impose the desired impedance model on the exosuit, the reference trajectory q_r can be updated by solving the impedance model (14), then the control objective is to drive the position q to track the reference position q_r. Thus, the adaptive control proposed in the subsection serves to track the reference trajectory q_r to enable the desired assistance performance between human and soft exosuit.

Since the dynamics of exosuit is invariant in each cycle due to the soft exosuit attached to human body and interacting with human with driven cables, and the tension torques in the cables can be compensated using the force load cell, therefore, the system parameters (such as inertia) are invariant in each iteration. Therefore, the inherent invariance such as the upper bound of robot dynamics could be exploited in the adaptive case [49]. It should be noted that these upper bounds can be estimated by a proposed updating law, not necessarily known in advance. Thus, position control of the exosuit motor can be achieved using the PD control (33) with a learning term that is composed of e_r and $\dot{e}_r$. Then, an adaptive position controller is developed such that $q \to q_r$ as $t \to \infty$.

The adaptive position controller can be designed as

$$\tau_m = K_p \tanh(e_r) + K_d \dot{e}_r - \mathrm{sgn}(r)\hat{\mathcal{K}} + F_m \tag{60}$$

where $\mathrm{sgn}(r) \in \mathbb{R}^{n\times n} = \mathrm{diag}[\mathrm{sgn}(r_1), \ldots, \mathrm{sgn}(r_n)]$, $\mathrm{sgn}(\cdot)$ denotes the sign function, e.g., $\mathrm{sgn}(r_i) = \frac{r_i}{\|r_i\|}$, and $\hat{\mathcal{K}} \in \mathbb{R}^n$ denotes the estimated value of $\mathcal{K} \in \mathbb{R}^n$. $\mathcal{K}$ is positive and $\|\mathcal{K}\| = k_M l_1 + k_C l_2^2 + k_G$, with l_1 and l_2 as the upper bounds of $\|\ddot{q}_r\|$ and $\|\dot{q}_r\|$, respectively. $\hat{\mathcal{K}}$ can be updated in each iteration according to

$$\dot{\hat{\mathcal{K}}} = -h(t)\Gamma \bar{r}\hat{\mathcal{K}} \tag{61}$$

where $\Gamma \in \mathbb{R}^{n\times n}$ is a known positive definite matrix, $\bar{r} \in \mathbb{R}^{n\times n} = \mathrm{diag}[r_1\mathrm{sgn}(r_1), \ldots, r_n\mathrm{sgn}(r_n)]$, and $h(t) = 1/(1+t)^2$ is a function of time which satisfies $h(t) > 0$ and $\lim_{t\to\infty} h(t) = 0$.

Substituting (60) into (6), the closed-loop dynamics can be described as follows:

$$\begin{aligned} &M(q)\ddot{q} + C(q,\dot{q})\dot{q} + \tau_f(\dot{q}) + G(q) - K_p \tanh(e_r) \\ &- K_d\dot{e}_r + \mathrm{sgn}(r)\hat{\mathcal{K}} = 0. \end{aligned} \tag{62}$$

Remark 4: Since the control design (60) utilizes the sign function, it would cause chattering in control torques. In order to eliminate such phenomenon, in actual experiments, we can replace it with the sat-function defined as follows:

$$\mathrm{sat}(\sigma) = \begin{cases} \mathrm{sgn}(\sigma), & \text{if } |\sigma| \geq \varsigma \\ \varsigma/\sigma, & \text{if } |\sigma| < \varsigma \end{cases}$$

where ς is the width of layer S_σ defined as $S_\sigma = \{|\sigma| < \varsigma\}$. When ς is small, despite the chattering appearing, the control tends to be robust, and the chattering shall disappear with the increase of ς, but the tracking performance would be worse and the tracking error would converge to a small set [50]. Therefore, we should make a tradeoff for the choice of ς.

Theorem 2: The developed controller (60) and the adaptive law (61) ensure the position tracking under the condition of given dynamics (6), i.e., $\lim_{t\to\infty} e_r(t) = 0$, and all the signals in the closed-loop system (62) are bounded if the controller gain K_p satisfies the following sufficient condition:

$$\begin{aligned} \lambda_{\min}\{\mu K_p\} > &\frac{\lambda_{\min}^2\{\mu K_d\}}{\zeta_2(\cosh^{-1}(\exp(\frac{\lambda_4}{\lambda_3}\|\delta(0)\|^2)+1)^2} \\ &+ \frac{{\zeta_0}^2(\cosh^{-1}(\exp(\frac{\lambda_4}{\lambda_3}\|\delta(0)\|^2)+1)^2}{\zeta_2} \\ &- \frac{\lambda_{\min}\{\mu K_d\}\zeta_0}{2\zeta_2(\cosh^{-1}(\exp(\frac{\lambda_4}{\lambda_3}\|\delta(0)\|^2)+1)} \end{aligned} \tag{63}$$

where $\zeta_2 = K_d - \zeta_1$, $\delta = [{e_r}^T, r^T, \tilde{\mathcal{K}}^T]^T$, $\delta(0)$ is the initial value of δ, and λ_3 and λ_4 are positive scalar constants selected as $\lambda_3 = \min\{\lambda_{\min}\{K_p\}, \frac{m_1}{2}\}$ and $\lambda_4 = \max\{\lambda_{\max}\{K_p\}, \frac{m_2}{2}\}$, respectively.

Proof: Define a Lyapunov function candidate as

$$V_2(t) = V_1(t) + \frac{1}{2}\tilde{\mathcal{K}}^T\Gamma^{-1}\tilde{\mathcal{K}} \tag{64}$$

where $\tilde{\mathcal{K}} = \hat{\mathcal{K}} - \mathcal{K}$.

Substituting (60) into (35), one has

$$\begin{aligned} M(q)\dot{r} = &-C(q,\dot{q})r + \psi_a\theta + K_p\tanh(e_r) \\ &+ K_d\dot{e}_r - \mathrm{sgn}(r)\hat{\mathcal{K}}. \end{aligned} \tag{65}$$

$V_2(t)$ can be bounded from (45) as follows:

$$\frac{1}{2}\lambda_3 \tanh^2(\|\mathcal{Y}\|) \leq V_2(t) \leq \lambda_4\|\delta\|^2. \tag{66}$$

After taking the time derivative of (64), we have

$$\begin{aligned} \dot{V}_2(t) = &r^T M(q)\dot{r} + \frac{1}{2}r^T\dot{M}_q r + \tanh^T(e_r)K_p\dot{e}_r \\ &+ \tilde{\mathcal{K}}^T\Gamma^{-1}\dot{\hat{\mathcal{K}}} \end{aligned} \tag{67}$$

where the fact $\dot{\tilde{\mathcal{K}}} = \dot{\hat{\mathcal{K}}}$ is used.

Furthermore, (67) can be simplified as

$$\begin{aligned} \dot{V}_2(t) = &-\tanh^T(e_r)\mu K_p\tanh(e_r) - r^T\mu K_d\tanh(e_r) \\ &- r^T K_d r + r^T\psi_a\theta - h(t)\tilde{\mathcal{K}}^T\bar{r}\hat{\mathcal{K}}. \end{aligned} \tag{68}$$

TABLE IV
SPECIFICATIONS OF THE SPRING GAUGE AND THE DAMPING ROD

Parameters	Ultimate load	Length	Weight	G_d
Spring	100 N	80mm	480g	1250N/m
Parameters	Ultimate load	Length	Weight	C_d
Damping	30 ∼ 600 N	40mm	270g	2600N/m/s

Since $-\tilde{\mathcal{K}}^T\hat{\mathcal{K}} \leqslant -(1/2)\tilde{\mathcal{K}}^T\tilde{\mathcal{K}} + (1/2)\mathcal{K}^T\mathcal{K}$, we can obtain that

$$\begin{aligned}\dot{V}_2(t) \leqslant & -\tanh^T(e_r)\mu K_p \tanh(e_r) - r^T\mu K_d \tanh(e_r) \\ & - r^T K_d r + r^T\psi_a\theta + \frac{1}{2}h(t)\mathcal{K}^T\bar{r}\mathcal{K} \\ & - \frac{1}{2}h(t)\tilde{\mathcal{K}}^T\bar{r}\tilde{\mathcal{K}}. \end{aligned} \tag{69}$$

Determined by the properties of $h(t)$, we can obtain that $\lim_{t\to\infty}(\frac{1}{2}h(t)\mathcal{K}^T\bar{r}\mathcal{K}) = 0$. As similar as (59), we can obtain that

$$\dot{V}_2(t) \leq -\beta_2 \tanh^2(\|\mathcal{Y}\|) \leq 0 \tag{70}$$

where β_2 is some positive constant related to Q in (51). K_p, K_d, and μ in Q should satisfy (53), (54), and (57) to make the matrix Q positive -definite. If the aforementioned condition is satisfied, when $e_r = 0$ and $r = 0$, we have $x = [0, 0]^T$ and $\mathcal{Y} = [0, 0]^T$, then $\|x\|^2 = 0$, $\tanh^2(\|\mathcal{Y}\|) = 0$, and $\dot{V}_2(t) = 0$ as $t \to \infty$; when $e_r \neq 0$ or $r \neq 0$, we have $x \neq [0, 0]^T$ and $\mathcal{Y} \neq [0, 0]^T$, then $\|x\|^2 > 0$, $\tanh^2(\|\mathcal{Y}\|) > 0$, and $\dot{V}_2(t) < 0$ as $t \to \infty$. Thus, we can obtain that $\dot{V}_2(t) < 0$ when $e_r, r \neq 0$ as $t \to \infty$. According to the Lyapunov stability criterion and the Barbalat's lemma, e_r and r can converge to 0 as $t \to \infty$. Furthermore, when $t \to \infty$, $V_2(t)$ is bounded by (66) when the inequality (63) is established, and $r(t)$ and $e_r(t)$ are also bounded, so we know from (34) that $\dot{e}_r$ is bounded. Given that the desired trajectory is bounded, e_r and $\dot{e}_r$ also bounded. Based on the aforementioned analysis, we know from (65) that $\dot{r}(t)$ is also bounded. It is easy to obtain that $\dot{\mathcal{Y}}(t)$ is bounded. ■

V. EXPERIMENTS VERIFICATION

A. Calibration Experiment

Before the experiment, a calibration step is necessary to render the impedance learning. To facilitate the impedance measurements of the human ankle, which is described by (14), an impedance calibration is performed depicted as follows. The calibration utilized the spring gauge and the damping rod with known impedance parameters, as shown in Table IV. In the stiffness experiment, one end of the spring gauge (developed by Guotai Gas Spring Technology Company, Ltd., Jiangsu, China) was fixed on the ground, and then, the Bowden cable was connected to the other end of the spring gauge, and the primal-dual model optimization is used to calculate the stiffness of the spring gauge. In the damping experiment, three damping rods (developed by Fuma Electronic Equipment Company, Ltd., Suzhou, China) were fixed and connected with two Bowden cables as the tension points of the system, and the damping coefficient of the damping rod was calculated. The experimental

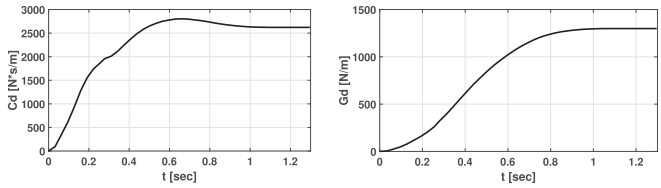

Fig. 5. Calibration experiments for impedance parameters. (Left) Parameter C_d of the damping rod. (Right) Parameter G_d of the spring gauge.

Fig. 6. Different terrains.

results shown in Fig. 5 indicate that the impedance parameters C_d and G_d gradually converge to actual values, which demonstrate the significance of the proposed optimization scheme.

Remark 5: In the experiment, the lower and upper bounds of $y = [\chi^T, \rho^T]^T$ are chosen properly, and χ should guarantee that the stiffness and damping values are gradually close to the true values of the participants on different terrains. Finally, $\chi^- = [\tilde{\mathcal{C}}_d^{-T}, \tilde{\mathcal{G}}_d^{-T}]^T = [-100N/(m/s), -100N/(m/s), -100N/m, -100N/m]^T$, and $\chi^+ = [\tilde{\mathcal{C}}_d^{+T}, \tilde{\mathcal{G}}_d^{+T}]^T = [100\,N/(m/s),\ 100\,N/(m/s), 100\,N/m,\ 100\,N/m]^T$. The bounds of dual decision vectors ρ are set as $-\varpi$ and ϖ. ϖ is large enough to replace $+\infty$ for the purpose of implementation convenience.

B. Terrains Experiments

The experiment demonstrates that the proposed impedance learning and hierarchical controller are accurate and stable, providing a smooth intervention when the users require assistance. It modulates the piece of torque at the human ankle according to the subject's movement capacity and reduces the muscular exertion during human locomotion. Several experiments were performed on different terrains, e.g., the plastic, the grassland, and the sands, to evaluate our proposed approach. Ethics Committee of Yueyang Hospital of integrated traditional Chinese and Western Medicine approved the experimental ethics document of Shanghai University of Traditional Chinese Medicine with reference number 2019-014. Three subjects are involved in the experiments, as shown in Fig. 6. The user's pieces of information is shown in Table V. The plastic terrain is the hardest among the three terrains, followed by the grass, and the sands (which we

TABLE V
HEIGHT AND WEIGHT OF THREE SUBJECTS

Subject	Height	Weight
S1	176 cm	63 kg
S2	175 cm	70 kg
S3	170 cm	73 kg

TABLE VI
VALUES OF COEFFICIENT USED IN THE EXPERIMENTS

Parameters	Plastic	Grassland	Sand
r_h	0.0475 m	0.0475 m	0.0475 m
r_a	0.13 m	0.13 m	0.13 m
l_a	0.22 m	0.22 m	0.22 m
γ	10^5	10^5	10^5
W_c	$\mathrm{diag}[0.6, 0.6]$	$\mathrm{diag}[0.6, 0.6]$	$\mathrm{diag}[0.6, 0.6]$
W_k	$\mathrm{diag}[0.4, 0.4]$	$\mathrm{diag}[0.4, 0.4]$	$\mathrm{diag}[0.4, 0.4]$
K_p	$\mathrm{diag}[20, 20]$	$\mathrm{diag}[23, 21]$	$\mathrm{diag}[23, 21]$
K_d	$\mathrm{diag}[4, 3]$	$\mathrm{diag}[4, 3]$	$\mathrm{diag}[3, 3]$
Γ	$\mathrm{diag}[0.3, 0.2]$	$\mathrm{diag}[0.3, 0.2]$	$\mathrm{diag}[0.3, 0.2]$
μ	$\mathrm{diag}[0.5, 0.5]$	$\mathrm{diag}[0.5, 0.5]$	$\mathrm{diag}[0.5, 0.5]$

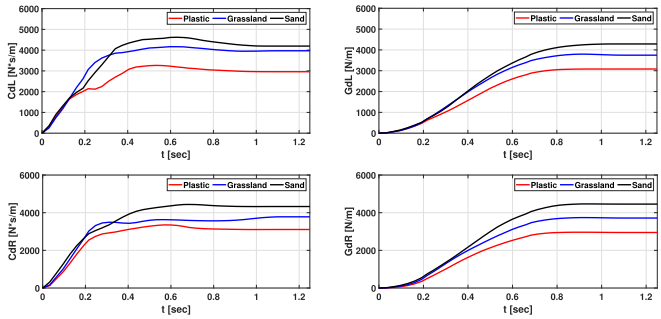

Fig. 7. Parameters C_d and G_d of the left ankle and right ankle of the first subject under three terrains.

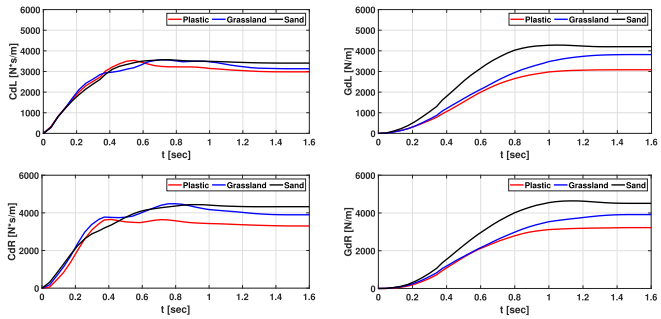

Fig. 8. Parameters C_d and G_d of the left ankle and right ankle of the first subject under three terrains where $W_c = W_k = \mathrm{diag}[1, 1]$.

renovated before experimenting because it just rained) are the softest. The chosen parameters in optimization and control are listed in Table VI.

C. Experimental Results

1) Impedance Learning: Results of impedance learning of the first subject with the assistance are depicted in Figs. 7–9, showing a clear increase in the amplitude of the impedance parameters when the exosuit assists the motion. Fig. 7 shows

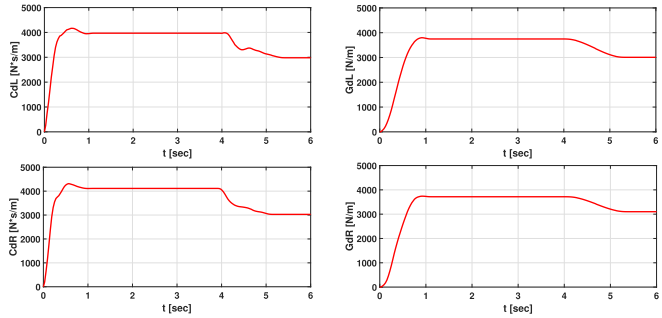

Fig. 9. Terrain conversion experimental result from grassland to plastic of the first subject.

the change of the impedance parameters of the first subject under the three terrains with $W_c = \mathrm{diag}[0.6, 0.6]$ and $W_k = \mathrm{diag}[0.4, 0.4]$. We can see that the stiffness parameter of the system G_d finally converges to a stable value within 1.2 s. The evolution of the damping parameter of the system is similar to the stiffness parameter. The experimental results show the desired interaction performance: the angle of ankle joint increases in the process of ankle lifting and the impedance parameter becomes larger. The impedance parameters converge to different values under different terrains. It indicates that the change of terrain leads to the change of human–environment interaction, which is an issue that the human–robot interaction control of soft exosuit has to consider. In order to explore the influence of parameters W_c and W_k on the impedance learning process, we set different values of parameters W_c and W_k. Fig. 8 shows the evolution of the impedance parameters of the first subject under three different terrains with $W_c = \mathrm{diag}[1, 1]$ and $W_k = \mathrm{diag}[1, 1]$, the convergence speed is smaller than that in Fig. 7. It means that the variety of parameters W_c and W_k can result in different convergence speed of impedance parameters. In addition, the terrain transformation experiment had been conducted. Fig. 9 depicts the changes in the first subject switched from the grassland to the plastic terrain. The figure shows that the impedance parameters converges to a stable value as the subjects step between the two different terrains, which indicates that the proposed impedance learning method can adapt to different terrains in a short time and has strong robustness.

From the aforementioned discussions, we have demonstrated the effectiveness and robustness of the impedance learning method, and the experimental results show that the softer the terrain surface, the larger the impedance parameters. That is, C_d and G_d would quickly converge to a larger value, respectively. When stepping over a different terrain, the impedance parameters would converge to another value, which verify that the proposed scheme has improved adaptability. The consistent conclusions can be drawn from the similar impedance learning results of the second and the third subject in the Appendixes A and B.

2) Controller Performance: The second experiment examines the efficacy of the developed controller in adapting its contribution to the subject's capacity of motion. The force sensor mounted on the foot can be used as a switching signal to change

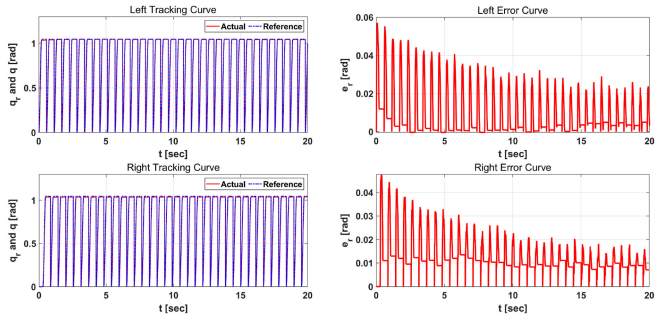

Fig. 10. Tracking trajectories and errors of the first subject on the plastic.

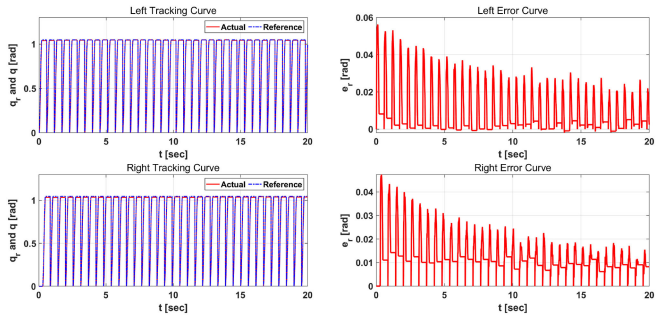

Fig. 11. Tracking trajectories and errors of the first subject on the grassland.

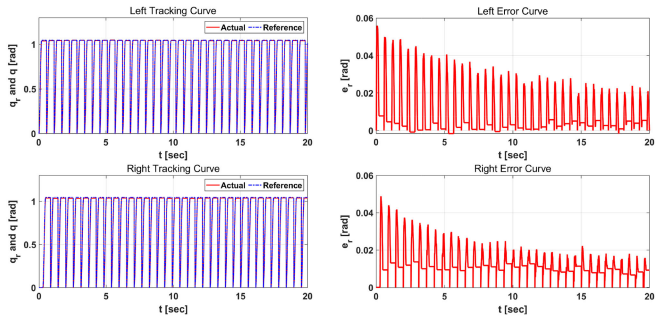

Fig. 12. Tracking trajectories and errors of the first subject on the sand.

the gait. When it is detected that the heel of one foot is on the ground, the motor on the other end is switched to the auxiliary phase, and the torque mode is activated to monitor the position and integral force. Conversely, when the forefoot on the assist phase side is off the ground, the motor on the same side is switched to the nonassisted mode and returns to the initial angle.

The proposed controller's tracking performance of the first subject was shown in Figs. 10–12, which includes the actual positions and the tracking errors. The top two subfigures are the curves for the left foot, and the bottom two subfigures are the curves for the right foot. It can be observed that the position errors of the left and right ankle joints are significantly reduced and converge in a small range. Fig. 13 shows the tracking performance of the adopted PD control for the first subject under the plastic terrain. From Figs. 10 and 13, it can be seen that the position errors have remained within a larger boundedness, and the PD control shows worse performance compared with the

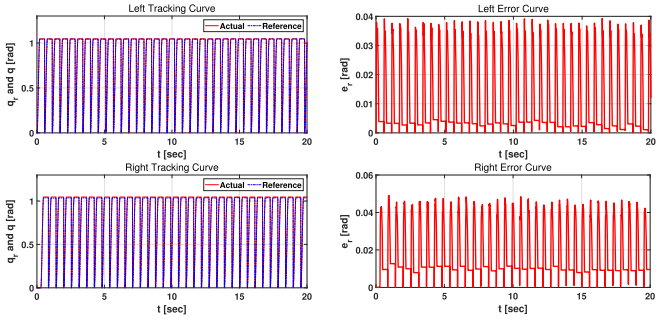

Fig. 13. Tracking trajectories and errors of the first subject with PD control on the plastic.

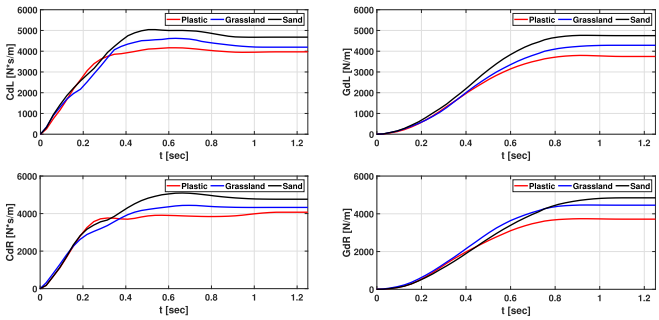

Fig. 14. Parameters C_d and G_d of the left ankle and right ankle of the second subject under three terrains.

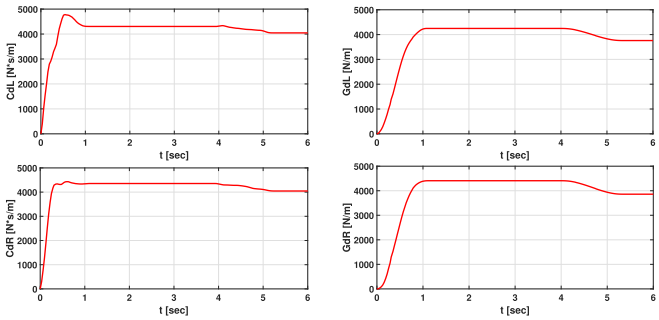

Fig. 15. Terrain conversion experimental result from grassland to plastic of the second subject.

proposed control, confirming that the controller has adapted to wearer's athletic ability to provide a greater assistance. It also proves that the control performance of the proposed controller is not affected by the impedance learning method, and they can be used independently as needed. The consistent conclusions can be drawn from the similar control performance results of the second and the third subject in the Appendices A and B.

This article proposed a novel strategy called optimized assist-as-needed paradigm, and as far as we know, it should be the first time that simultaneous optimization and control are considered for a exosuit. The subjects want compliant intervention from the controller when wearing the soft exosuit. It can adjust the output of impedance learning based on the target dynamics in multiple environments. The presented prototype has proved the feasibility of our suggested optimization and control structure. Based on

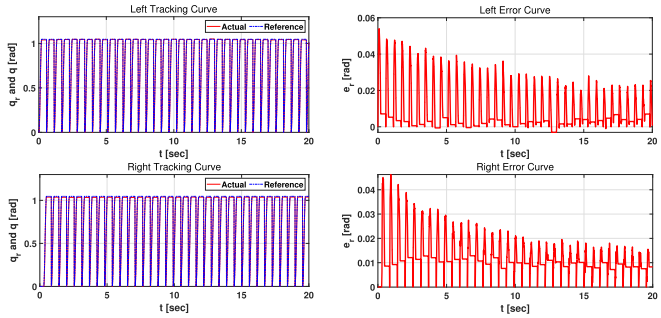

Fig. 16. Tracking trajectories and errors of the second subject on the plastic.

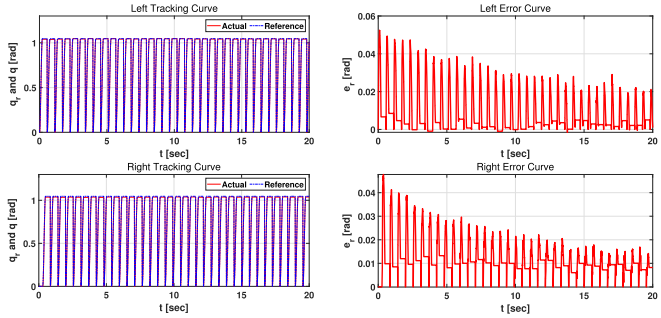

Fig. 17. Tracking trajectories and errors of the second subject on the grassland.

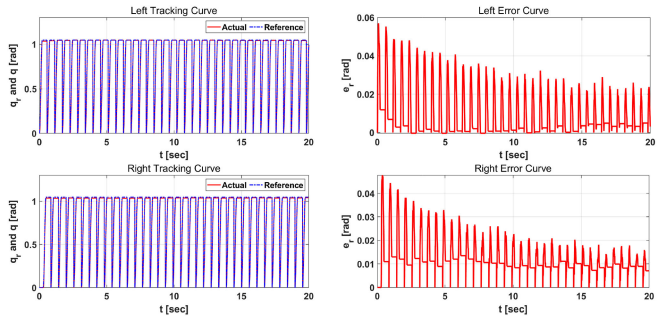

Fig. 18. Tracking trajectories and errors of the second subject on the sand.

this work, the scheme can be extended to other multijoints (such as wrist, ankle, and hip), as well as the actuation frame of the whole-body exosuit. In this article, we develop the suit and assess its performance with the physiology and morphology of the user, then spread it to multiple users.

VI. Conclusion

In this article, impedance learning and human-in-the-loop adaptive control framework for the soft exosuit to interact with different terrains were investigated. A novel hierarchical human-in-the-loop paradigm was formulated to produce suitable assistance powers to the cable-driven lower limb exosuits for aiding the human ankle joint pushing off the ground. In order to optimize the impedance parameters under different terrains, its impedance model can be transferred to a QP problem with

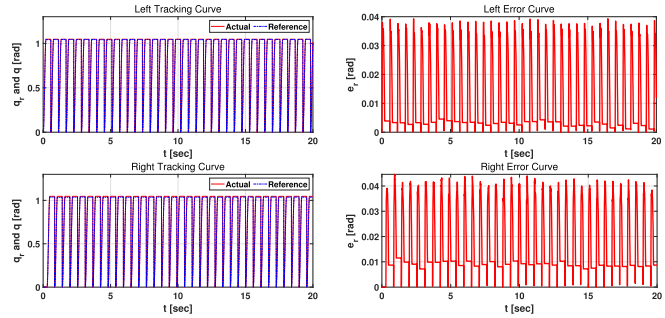

Fig. 19. Tracking trajectories and errors of the second subject with PD control on the plastic.

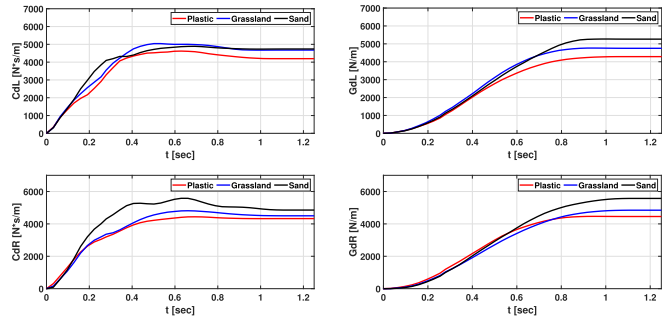

Fig. 20. Parameters C_d and G_d of the left ankle and right ankle of the third subject under three terrains.

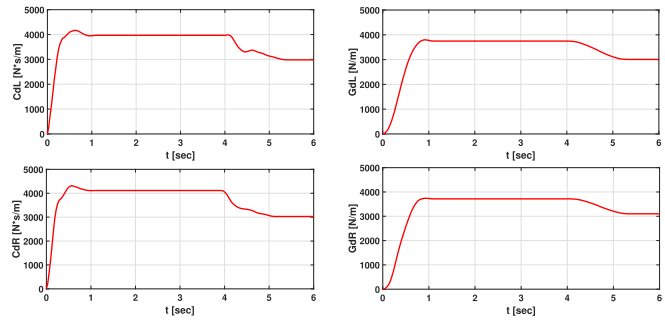

Fig. 21. Terrain conversion experimental result from grassland to plastic of the third subject.

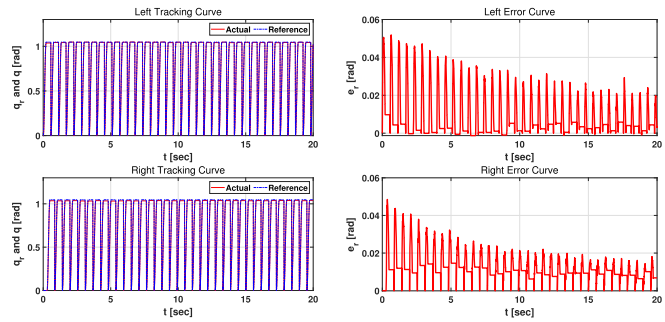

Fig. 22. Tracking trajectories and errors of the third subject on the plastic.

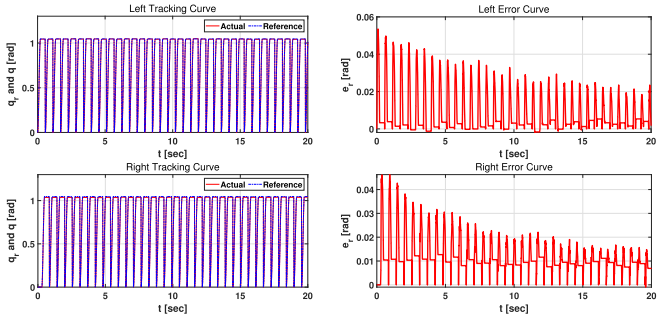

Fig. 23. Tracking trajectories and errors of the third subject on the grassland.

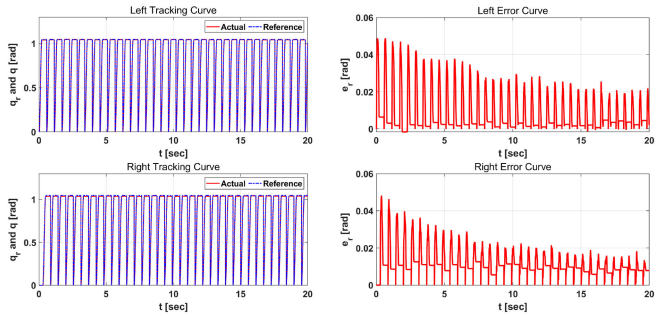

Fig. 24. Tracking trajectories and errors of the third subject on the sand.

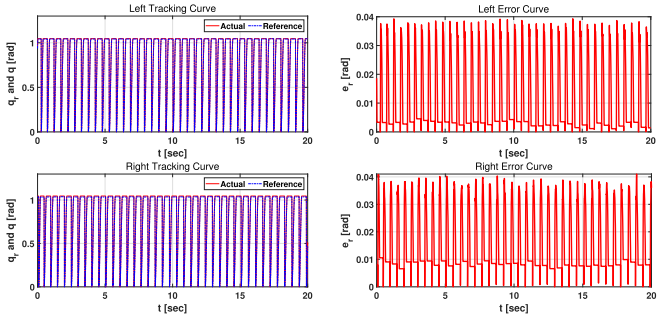

Fig. 25. Tracking trajectories and errors of the third subject with PD control on the plastic.

specified constraints, and then, it was solved by a designed primal-dual optimization model. Then, the proposed impedance learning can adapt the impedance model to regulate the assistance forces for humans on different terrains. Then, an adaptive controller was exploited to balance the nonlinearities and compliance factors existing in the human-exosuit interaction, while the robust mechanism compensates for disturbances. The feasibility and effectiveness of the proposed method were verified through comparative experiments under different terrains. In future work, we would consider extending the proposed optimized assist-as-needed strategy to multi-joints actuated soft exosuit.

APPENDIX A

The experimental results of the second subject: Figs. 14 and 15 show the impedance learning results. Figs. 16–18 show the proposed controller performance on three terrains. The top two subfigures are the curves for the left foot, and the bottom two subfigures are the curves for the right foot. Fig. 19 shows the tracking performance of the PD controller on the plastic.

APPENDIX B

The experimental results of the third subject: Figs. 20 and 21 show the impedance learning results. Figs. 22–24 demonstrate the performance of the trajectory tracking on three different terrains. The top two subfigures are the curves for the left foot, and the bottom two subfigures are the curves for the right foot. Fig. 25 shows the tracking performance of the PD controller on the plastic.

REFERENCES

[1] L. M. Mooney, E. J. Rouse, and H. M. Herr, "Autonomous exoskeleton reduces metabolic cost of human walking during load carriage," *J. Neuroeng. Rehabil.*, vol. 11, no. 1, pp. 1–11, 2014.

[2] L. Xie, G. Huang, L. Huang, S. Cai, and X. Li, "An unpowered flexible lower limb exoskeleton: Walking assisting and energy harvesting," *IEEE/ASME Trans. Mechatron.*, vol. 24, no. 5, pp. 2236–2247, Oct. 2019.

[3] G. Orekhov, Y. Fang, J. Luque, and Z. F. Lerner, "Ankle exoskeleton assistance can improve over-ground walking economy in individuals with cerebral palsy," *IEEE Trans. Neural Syst. Rehabil. Eng.*, vol. 28, no. 2, pp. 461–467, Feb. 2020.

[4] W. Huo, S. Mohammed, J. C. Moreno, and Y. Amirat, "Lower limb wearable robots for assistance and rehabilitation: A state of the art," *IEEE Syst. J.*, vol. 10, no. 3, pp. 1068–1081, Sep. 2016.

[5] I. Farkhatdinov, J. Ebert, G. van Oort, M. Vlutters, E. van Asseldonk, and E. Burdet, "Assisting human balance in standing with a robotic exoskeleton," *IEEE Robot. Automat. Lett.*, vol. 4, no. 2, pp. 414–421, Apr. 2019.

[6] L. Zhou, W. Chen, J. Wang, S. Bai, H. Yu, and Y. Zhang, "A novel precision measuring parallel mechanism for the closed-loop control of a biologically inspired lower limb exoskeleton," *IEEE/ASME Trans. Mechatron.*, vol. 23, no. 6, pp. 2693–2703, Dec. 2018.

[7] O. M. Alaoui, F. Expert, G. Morel, and N. Jarrasse, "Using generic upper-body movement strategies in a free walking setting to detect gait initiation intention in a lower-limb exoskeleton," *IEEE Trans. Med. Robot. Bionics*, vol. 2, no. 2, pp. 236–247, May 2020.

[8] E. IdÃ, T. Bruckmann, and M. Carricato, "Rest-to-rest trajectory planning for underactuated cable-driven parallel robots," *IEEE Trans. Robot.*, vol. 35, no. 6, pp. 1338–1351, Dec. 2019.

[9] A. T. Asbeck, S. M. M. De Rossi, I. Galiana, Y. Ding, and C. J. Walsh, "Stronger, smarter, softer: Next-generation wearable robots," *IEEE Robot. Autom. Mag.*, vol. 21, no. 4, pp. 22–33, Dec. 2014.

[10] Y. Ding *et al.*, "Biomechanical and physiological evaluation of multi-joint assistance with soft exosuits," *IEEE Trans. Neural Syst. Rehabil. Eng.*, vol. 25, no. 2, pp. 119–130, Feb. 2017.

[11] S. H. Collins, M. B. Wiggin, and G. S. Sawicki, "Reducing the energy cost of human walking using an unpowered exoskeleton," *Nature*, vol. 522, no. 7555, pp. 212–215, 2015.

[12] E. J. Park *et al.*, "A hinge-free, non-restrictive, lightweight tethered exosuit for knee extension assistance during walking," *IEEE Trans. Med. Robot. Bionics*, vol. 2, no. 2, pp. 165–175, May. 2020.

[13] M. B. Yandell, J. R. Tacca, and K. E. Zelik, "Design of a low profile, unpowered ankle exoskeleton that fits under clothes: Overcoming practical barriers to widespread societal adoption," *IEEE Trans. Neural Syst. Rehabil. Eng.*, vol. 27, no. 4, pp. 712–723, Apr. 2019.

[14] F. A. Panizzolo *et al.*, "Lower limb biomechanical analysis during an unanticipated step on a bump reveals specific adaptations of walking on uneven terrains," *J. Exp. Biol.*, vol. 220, no. 22, pp. 4169–4176, 2017.

[15] J. Sanchez-Sanchez *et al.*, "Effect of natural turf, artificial turf, and sand surfaces on sprint performance: A systematic review and meta-analysis," *Int. J. Environ. Res. Public Health*, vol. 17, no. 24, pp. 1–12, 2020.

[16] H. Modares, I. Ranatunga, F. L. Lewis, and D. O. Popa, "Optimized assistive human–robot interaction using reinforcement learning," *IEEE Trans. Cybern.*, vol. 46, no. 3, pp. 655–667, Mar. 2016.

[17] C. Yang, G. Ganesh, S. Haddadin, S. Parusel, A. Albu-Schaeffer, and E. Burdet, "Human-like adaptation of force and impedance in stable and unstable interactions," *IEEE Trans. Robot.*, vol. 27, no. 5, pp. 918–930, Oct. 2011.
[18] L. Rozo, S. Calinon, D. G. Caldwell, P. Jiménez, and C. Torras, "Learning physical collaborative robot behaviors from human demonstrations," *IEEE Trans. Robot.*, vol. 32, no. 3, pp. 513–527, Jun. 2016.
[19] T. G. Thuruthel, E. Falotico, F. Renda, and C. Laschi, "Model-based reinforcement learning for closed-loop dynamic control of soft robotic manipulators," *IEEE Trans. Robot.*, vol. 35, no. 1, pp. 124–134, Feb. 2019.
[20] O. Koç, G. Maeda, and J. Peters, "Optimizing the execution of dynamic robot movements with learning control," *IEEE Trans. Robot.*, vol. 35, no. 4, pp. 909–924, Aug. 2019.
[21] B. Kim, J. Park, S. Park, and S. Kang, "Impedance learning for robotic contact tasks using natural actor-critic algorithm," *IEEE Trans. Syst., Man, Cybern. B, Cybern.*, vol. 40, no. 2, pp. 433–443, Apr. 2010.
[22] C. Yang, C. Zeng, C. Fang, W. He, and Z. Li, "A DMPs-based framework for robot learning and generalization of humanlike variable impedance skills," *IEEE/ASME Trans. Mechatron.*, vol. 23, no. 3, pp. 1193–1203, Jun. 2018.
[23] G. Peng, C. Yang, W. He, and C. L. P. Chen, "Force sensorless admittance control with neural learning for robots with actuator saturation," *IEEE Trans. Ind. Electron.*, vol. 67, no. 4, pp. 3138–3148, Apr. 2020.
[24] W. Sun, J.-W. Lin, S.-F. Su, N. Wang, and M. J. Er, "Reduced adaptive fuzzy decoupling control for lower limb exoskeleton," *IEEE Trans. Cybern.*, vol. 51, no, 3, pp. 1099–1109, Mar. 2021.
[25] J. Wang and O. R. Barry, "Inverse optimal robust adaptive controller for upper limb rehabilitation exoskeletons with inertia and load uncertainties," *IEEE Robot. Automat. Lett.*, vol. 6, no. 2, pp. 2171–2178, Apr. 2021.
[26] B. Brahmi, M. Saad, C. Ochoa-Luna, M. H. Rahman, and A. Brahmi, "Adaptive tracking control of an exoskeleton robot with uncertain dynamics based on estimated time-delay control," *IEEE/ASME Trans. Mechatron.*, vol. 23, no. 2, pp. 575–585, Apr. 2018.
[27] Z. Li and C.-Y. Su, "Neural-adaptive control of single-master multiple slaves teleoperation for coordinated multiple mobile manipulators with time-varying communication delays and input uncertainty," *IEEE Trans. Neural Netw. Learn. Syst.*, vol. 24, no. 9, pp. 1400–1413, Sep. 2013.
[28] Z. Li, J. Li, and Y. Kang, "Adaptive robust coordinated control of multiple mobile manipulators interacting with rigid environments," *Automatica*, vol. 46, no. 12, pp. 2028–2034, 2010.
[29] B. K. Dinh, M. Xiloyannis, C. W. Antuvan, L. Cappello, and L. Masia, "Hierarchical cascade controller for assistance modulation in a soft wearable arm exoskeleton," *IEEE Robot. Automat. Lett.*, vol. 2, no. 3, pp. 1786–1793, Jul. 2017.
[30] B. T. Quinlivan *et al.*, "Assistance magnitude versus metabolic cost reductions for a tethered multiarticular soft exosuit," *Sci. Robot.*, vol. 2, no. 2, pp. 1–17, 2017.
[31] G. Lee, Y. Ding, I. G. Bujanda, N. Karavas, Y. M. Zhou, and C. J. Walsh, "Improved assistive profile tracking of soft exosuits for walking and jogging with off-board actuation," in *Proc. IEEE Int. Conf. Intell. Robots Syst.*, 2017, pp. 1699–1706.
[32] M. Xiloyannis, D. Chiaradia, A. Frisoli, and L. Masia, "Physiological and kinematic effects of a soft exosuit on arm movements," *J. NeuroEng. Rehabil.*, vol. 16, no. 1, pp. 1–15, 2019.
[33] M. Xiloyannis *et al.*, "Soft robotic suits: State of the art, core technologies, and open challenges," *IEEE Trans. Robot.*, early access, Jun. 2021, doi: 10.1109/TRO.2021.3084466.
[34] H. Lee and N. Hogan, "Time-varying ankle mechanical impedance during human locomotion," *IEEE Trans. Neural Syst. Rehabil. Eng.*, vol. 23, no. 5, pp. 755–764, Sep. 2015.
[35] H. Lee, E. J. Rouse, and H. I. Krebs, "Summary of human ankle mechanical impedance during walking," *IEEE J. Trans. Eng. Health Med.*, vol. 4, pp. 1–7, 2016.
[36] A. L. Shorter and E. J. Rouse, "Mechanical impedance of the ankle during the terminal stance phase of walking," *IEEE Trans. Neural Syst. Rehabil. Eng.*, vol. 26, no. 1, pp. 135–143, Jan. 2018.
[37] G. M. Gasparri, J. Luque, and Z. F. Lerner, "Proportional joint-moment control for instantaneously adaptive ankle exoskeleton assistance," *IEEE Trans. Neural Syst. Rehabil. Eng.*, vol. 27, no. 4, pp. 751–759, Apr. 2019.
[38] F. L. Lewis, D. M. Dawson, and C. T. Abdallah, *Robot Manipulator Control: Theory and Practice*, 2nd ed. New York, NY, USA: Marcel Dekker, 2004.
[39] L. Sciavicco and B. Siciliano, *Modelling and Control of Robot Manipulators*, 2nd ed. London, U.K.: Springer-Verlag, 2000.
[40] S. Nicosia and P. Tomei, "A tracking controller for flexible joint robots using only link position feedback," *IEEE Trans. Autom. Control*, vol. 40, no. 5, pp. 885–890, May 1995.
[41] Y. Lin, Z. Chen, and B. Yao, "Unified method for task-space motion/force/impedance control of manipulator with unknown contact reaction strategy," *IEEE Robot. Automat. Lett.*, vol. 7, no. 2, pp. 1478–1485, Apr. 2022.
[42] D. Erickson, M. Weber, and I. Sharf, "Contact stiffness and damping estimation for robotic systems," *Int. J. Robot. Res.*, vol. 22, no. 1, pp. 41–57, 2003.
[43] Y. Zhang, S. S. Ge, and T. H. Lee, "A unified quadratic-programming-based dynamical system approach to joint torque optimization of physically constrained redundant manipulators," *IEEE Trans. Syst., Man, Cybern. B, Cybern.*, vol. 34, no. 5, pp. 2126–2132, Oct. 2004.
[44] Z. Li, S. S. Ge, and S. Liu, "Contact-force distribution optimization and control for quadruped robots using both gradient and adaptive neural networks," *IEEE Trans. Neural Netw. Learn. Syst.*, vol. 25, no. 8, pp. 1460–1473, Aug. 2014.
[45] F.-T. Cheng, R.-J. Sheu, and T.-H. Chen, "The improved compact QP method for resolving manipulator redundancy," *IEEE Trans. Syst., Man, Cybern.* vol. 25, no. 11, pp. 1521–1530, Nov. 1995.
[46] K. Dalamagkidis, K. P. Valavanis, and L. A. Piegl, "Nonlinear model predictive control with neural network optimization for autonomous autorotation of small unmanned helicopters," *IEEE Trans. Control Syst. Technol.*, vol. 19, no. 4, pp. 818–831, Jul. 2011.
[47] N. Sadegh and R. Horowitz, "Stability and robustness analysis of a class of adaptive controllers for robotic manipulators," *Int. J. Robot. Res.*, vol. 9, no. 9, pp. 74–92, 1990.
[48] W. E. Dixon, M. S. de Queiroz, F. Zhang, and D. M. Dawson, "Tracking control of robot manipulators with bounded torque inputs," *Robotica*, vol. 17, no. 2, pp. 121–129, 1999.
[49] Y. Li and S. S. Ge, "Impedance learning for robots interacting with unknown environments," *IEEE Trans. Control Syst. Technol.*, vol. 22, no. 4, pp. 1422–1432, Jul. 2014.
[50] J. J. Slotine and W. Li, *Applied Nonlinear Control*. Hoboken, NJ, USA: Prentice Hall, 1991.

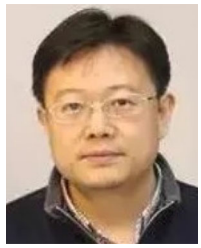

Zhijun Li (Fellow, IEEE) received the Ph.D. degree in mechatronics from Shanghai Jiao Tong University, Shanghai, China, in 2002.

From 2003 to 2005, he was a Postdoctoral Fellow with the Department of Mechanical Engineering and Intelligent Systems, The University of Electro-Communications, Tokyo, Japan. From 2005 to 2006, he was a Research Fellow with the Department of Electrical and Computer Engineering, National University of Singapore, Singapore, and Nanyang Technological University, Singapore. Since 2017, he has been a Professor with the Department of Automation, University of Science and Technology, Hefei, China, where he has been the Vice Dean with the School of Information Science and Technology since 2019. His current research interests include wearable robotics, biomechatronics systems, nonlinear control, and computational optimization.

Dr. Li has been the Co-Chair of IEEE SMC Technical Committee on Bio-Mechatronics and Bio-Robotics Systems, and IEEE RAS Technical Committee on Neuro-Robotics Systems. He is serving as a Senior Editor for *Journal of Intelligent & Robotic Systems*, and an Associate Editor for several IEEE Transactions.

Xiang Li received the B.S. degree in automation from the Anhui University of Technology, Maanshan, China, in 2019. He is currently working toward the M.S. degree in control engineering with the University of Science and Technology of China, Hefei, China.

His current research interests include adaptive control and nonlinear control of exoskeleton and soft exosuits.

Qinjian Li received the B.S. degree in automation from the Nanjing Institute of Technology, Nanjing, China, in 2015. He is currently working toward the Ph.D. degree in control science and engineering with the University of Science and Technology of China, Hefei, China.

His current research interests include the design and control of soft exosuits and robotic leg prostheses.

Hang Su (Member, IEEE) received the M.Sc. degree in control theory and control engineering from the South China University of Technology, Guangzhou, China, in 2015, and the Ph.D. degree in bioengineering from Politecnico di Milano, Milano, Italy, in 2019.

He has authored and coauthored more than 70 papers in international journals and conferences. His main research interests include control and instrumentation in medical robotics, human–robot interaction, sensor fusions, deep learning, and bilateral teleoperation.

Dr. Su is currently an Associate Editor for *Frontiers in Neurorobotics and Frontiers in Neuroscience*. He serve as a Program Chair for the IEEE International Conference on Advanced Robotics and Mechatronics (ICARM 2022/2021). He also serves as the Associate Editor for IEEE International Conference on Robotics and Automation (ICRA) and IEEE/RSJ International Conference on Intelligent Robots and Systems, IEEE International Conference on Robot and Human Interactive Communication, and the ICARM, and the Guest Associate Editor for a couple of journals. He was the recipient of the 2021 Andrew P. Sage Best Transactions Paper Award on IEEE TRANSACTIONS ON HUMAN-MACHINE SYSTEMS, the Best Conference Paper Award in Advanced Robotics at IEEE International Conference on Advanced Robotics and Mechatronics in 2020, and the ICRA Travel Award funded by IEEE Robotics and Automation Society in 2019.

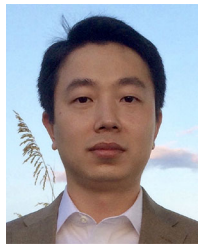

Zhen Kan (Member, IEEE) received the Ph.D. degree in mechanical engineering from the Department of Mechanical and Aerospace Engineering, University of Florida, Gainesville, FL, USA, in 2011.

He was a Postdoctoral Research Fellow with the Air Force Research Laboratory, Eglin AFB and the University of Florida Research and Engineering Education Facility, from 2012 to 2016, and was an Assistant Professor with the Department of Mechanical Engineering, University of Iowa, from 2016 to 2019. He is currently a Professor with the Department of Automation, University of Science and Technology of China, Hefei, China. His research interests include networked control systems, nonlinear control, formal methods, and robotics.

Dr. Kan currently serves on program committees of several internationally recognized scientific and engineering conferences and is an Associate Editor for IEEE TRANSACTIONS ON AUTOMATIC CONTROL.

Wei He (Senior Member, IEEE) received the B.Eng. degree in automation and M.Eng. degree in control science and engineering from the College of Automation Science and Engineering, South China University of Technology, Guangzhou, China, in 2006 and 2008, respectively, and the Ph.D. degree in control science and engineering from the Department of Electrical and Computer Engineering, National University of Singapore, Singapore, in 2011 .

He is currently working as a Full Professor with the Institute of Artificial Intelligence and School of Automation and Electrical Engineering, University of Science and Technology Beijing, Beijing, China. He has coauthored three books published in Springer and authored/coauthored more than 200 international journal and conference papers. His current research interests include robotics, distributed parameter systems, and intelligent control systems.

Dr. He is serving as the Chair of IEEE SMC Society Beijing Capital Region Chapter. He is serving as an Associate Editor for IEEE TRANSACTIONS ON ROBOTICS, IEEE TRANSACTIONS ON NEURAL NETWORKS AND LEARNING SYSTEMS, IEEE TRANSACTIONS ON CONTROL SYSTEMS TECHNOLOGY, *Science China Information Sciences*, and IEEE/CAA JOURNAL OF AUTOMATICA SINICA.